

## Measurement of Pressure-Gradient-Driven Currents in Tokamak Edge Plasmas

D. M. Thomas, A. W. Leonard, L. L. Lao, and T. H. Osborne  
*General Atomics, P.O. Box 85608, San Diego, California 92186-5608, USA*

H. W. Mueller  
*Max Planck Institut für Plasma Physik, Garching, D-85748 Germany*

D. F. Finkenthal  
*Palomar College, San Marcos, California, 92069 USA*  
(Received 7 November 2003; published 6 August 2004)

Localized currents driven by pressure gradients play a pivotal role in the magnetohydrodynamic stability of toroidal plasma confinement devices. We have measured the currents generated in the edge of  $L$ - (low) and  $H$ - (high confinement) mode discharges on the DIII-D tokamak, utilizing the Zeeman effect in an injected lithium beam to obtain high resolution profiles of the poloidal magnetic field. We find current densities in excess of  $1 \text{ MA/m}^2$  in a 1 to 2 cm region near the peak of the edge pressure gradient. These values are sufficient to challenge edge stability theories based on specific current formation models.

DOI: 10.1103/PhysRevLett.93.065003

PACS numbers: 52.70.Ds, 52.55.Fa, 52.55.Tn, 52.70.Kz

In order to optimize the performance of magnetically confined fusion plasmas, it is important to understand the stability limits of the pedestal or edge region. This in turn requires an accurate knowledge of the currents in this region. According to theory, the high pressure gradients achieved in the edge of  $H$ - (high confinement) mode plasmas should lead to the generation of a significant edge current density peak through the bootstrap [1,2] and Pfirsch-Schlüter effects. Previous work has established the importance of the edge current density  $j(r)$  in the achievement of so-called “second stability” in the context of coupled magnetohydrodynamic (MHD) modes which are both pressure (ballooning) and current (peeling) driven [3–5]. Experimentally, Osborne *et al.* [6] observed that the value of the edge pressure gradient could exceed the calculated infinite toroidal mode number first stability limits by a factor of 2 for specifically shaped tokamak discharges and he argued that this difference could be accounted for if an edge current density peak opened access to a second stability.

Recent work has strengthened the connection between edge stability and an edge current density peak. It has been shown [7] that variations in edge localized mode (ELM) properties could be explained in terms of a low  $n$  toroidal mode number MHD model taking into account a second stable access because of an edge current density peak, and that this model could account for most features of ELMs in both the DIII-D and JT-60U tokamaks [8]. The development of a detailed model by Snyder *et al.* [9,10] and associated MHD stability code (ELITE) based on coupled peeling-ballooning modes has succeeded in describing many aspects of the pedestal including ELMs. For a given current distribution one is able to efficiently

calculate the stability and growth of the relevant modes for a broad range of plasma parameters [11].

This theoretical work, while very successful in constructing a picture of edge stability in accord with experimental observations, nevertheless rests on the presumption of a large edge current density peak that has not been directly measured until now. While there is a common practice of calculating the edge current density peak from the bootstrap effect [10,11], the theory of the bootstrap current at the edge is basically incorrect. The theory assumes  $\rho_\theta/L \ll 1$ , where  $\rho_\theta$  is the poloidal ion gyroradius and  $L$  is the relevant gradient scale length. In the tokamak edge  $\rho_\theta/L \sim 1$ . Although magnetic measurements including motional Stark effect (MSE) data indicate the presence of some current near the edge, the exact shape and magnitude of this current have been difficult to accurately determine. For the measured pressure profiles found in DIII-D, estimates of the edge current density profile constrained by the existing magnetic diagnostic set and the EFIT equilibrium reconstruction code [12] are roughly consistent with the stability limits set by the ELITE code calculations and are typically in the range of 0.5 to 1.0  $\text{MA/m}^2$ .

In this Letter, we report the first direct measurements of an edge current density peak in a tokamak with sufficient accuracy and spatial resolution to confirm this key element of the stability theory and test the accuracy of models used for calculating it. We do this by making a precise determination of the magnetic field structure *in situ* using an atomic beam probe. Measurements on DIII-D discharges having a variety of edge pressure gradients have yielded peak current densities in excess of  $1 \text{ MA/m}^2$  in the case of ELM-free  $H$ -mode discharges,

with the current localized to a narrow band in the vicinity of the peak of the pressure gradient.

The magnetic field measurements are made using the DIII-D LIBEAM system [13–15], a diagnostic which exploits the Zeeman effect in lithium. Because of the negligible Stark mixing of the relevant atomic levels in lithium, this method of determining  $j(r)$  is insensitive to the large local electric fields typically found in enhanced confinement ( $H$ -mode) edges, and thus avoids an ambiguity common to MSE measurements of internal magnetic fields. Figure 1 gives a detailed description of the installation and technique. Briefly, a 30 keV neutral lithium beam is injected into the edge of the plasma where it is collisionally excited. The emission of the  $2S-2P$  resonance line is both split and polarized by the tokamak magnetic field. By doing polarization analysis of one of the  $\sigma$  line components at multiple closely spaced locations along the beam, one can obtain direct information on the local magnetic field. Specifically, the diagnostic yields an array of 32 finely spaced ( $\Delta R \sim 0.5$  cm) values

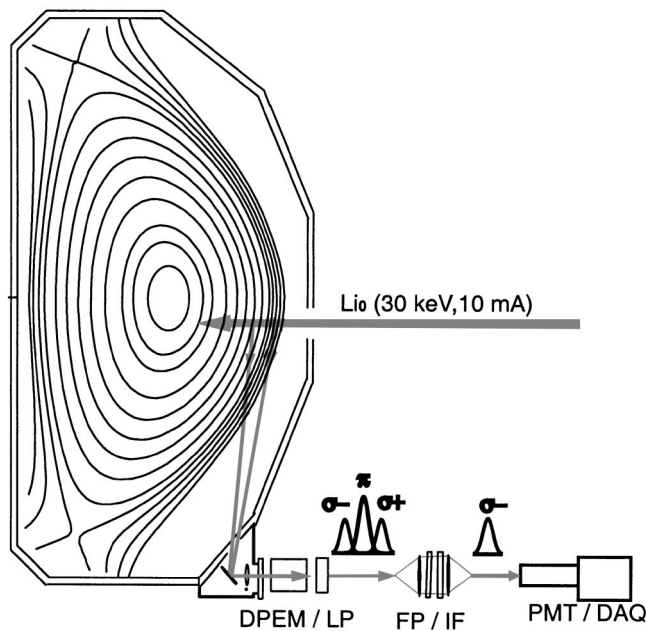


FIG. 1. Experimental setup. The 670 nm resonance fluorescence light from the collisionally excited beam is imaged at a series of closely spaced locations in the plasma edge. The polarization state of the  $\sigma^-$  Zeeman sublevel is analyzed by passing the light through dual photoelastic modulators (DPEM) and a linear polarizer (LP) to amplitude modulate the emission, which is detected by a bank of 32 photomultiplier tubes (PMT). Individually tuned etalon pairs (FP) and an interference filter (IF) isolate the  $\sigma^-$  component for each of the Doppler-shifted viewing locations. Digital lock-in analysis at the first and second PEM harmonics recovers the circular and linearly polarized fractions of the  $\sigma^-$  component; their ratio determines the magnitude of  $\cos(\alpha_{\text{VIEW}})$ , where  $\alpha_{\text{VIEW}}$  is the angle between the local magnetic field and each sight line.

of  $\cos(\alpha_{\text{VIEW}})$ , where  $\alpha_{\text{VIEW}}$  is the angle between the local magnetic field and each sight line. Multiplication of  $\cos(\alpha_{\text{VIEW}})$  by the total field yields  $B_{\text{VIEW}}$ , the magnetic field component parallel to the sight line. A spatial calibration allows us to decompose each measurement into vertical and radial magnetic field components  $\{B_r, B_z\}$  at the intersection of the sight lines and the injected beam, or a geometric projection of the standard magnetic pitch angle  $\gamma = \text{atan}(B_{\text{Pol}}/B_{\text{Tor}})$  where  $B_{\text{Pol}}$  and  $B_{\text{Tor}}$  are the tokamak poloidal and toroidal magnetic fields. These values may be used directly as new constraints in EFIT in order to improve the reconstruction of the plasma flux surfaces and current density profile. Alternatively, if we presume an approximate shape for the flux surfaces, the measured  $B_{\text{VIEW}}$  profile and its radial derivative can be used to infer the local current distribution directly using Ampère's law [16].

Figure 2 shows the time traces of several plasma parameters for DIII-D shot 115114, a high triangularity discharge for which there was a relatively long ELM-free period and a corresponding large increase in the edge pressure gradient. In Fig. 3 we compare the measured pitch angle projections during the  $L$ -mode and  $H$ -mode phases of this shot with those calculated from EFIT using the existing magnetic coil and MSE inputs (i.e., without using the LIBEAM data). The EFIT values are obtained by reconstructing the proper direction cosines from the known spatial calibration and the

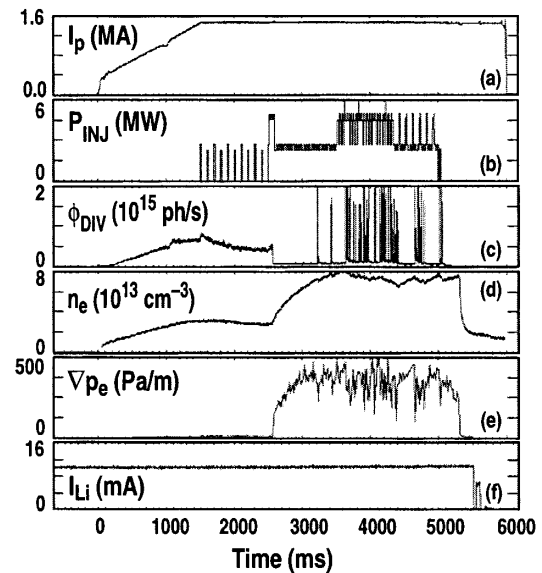


FIG. 2. Time trace of plasma parameters for shot 115114 showing (a) plasma current, (b) injected neutral beam power, (c) divertor  $D_\alpha$  emission, (d) line-averaged electron density, (e) maximum edge electron pressure gradient (from Thomson scattering), and (f) lithium beam current. The  $L$ -to- $H$  transition occurs at 2598 ms.  $L$ -mode data were acquired from 2250 to 2340 ms,  $H$  mode from 3065 to 3215 ms during the ELM-free phase.

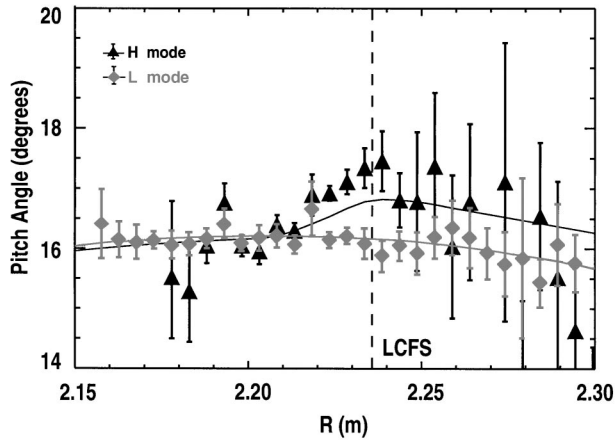


FIG. 3. Comparison of the calculated magnetic pitch angle profile  $\gamma$  versus major radius  $R$  from an EFIT reconstruction projected into the LIBEAM view chords with a measured profile from the diagnostic for shot 115114 during  $L$ -mode phase (gray) and late  $H$ -mode phase just before the collapse of the pedestal pressure (black). The error bars represent statistical uncertainty for each point combined with an estimated systematic calibration error. Position of the last closed flux surface in the trajectory of the beam is indicated by the dashed vertical line. Averaging time in the  $L$ -mode case is 100 ms and for the  $H$ -mode phases 150 ms. The large increase in the  $H$ -mode error bars at the two extremes of the array are due to low signals: on the outside due to the drop in plasma density and on the inside due to beam attenuation.

calculated  $\{B_r, B_z\}$  values at the same time as the  $L$ -mode data. During the  $L$ -mode phase the plasma pressure is quite low, and one would expect very low edge current. Under these conditions, the EFIT reconstructions are particularly well constrained and we find excellent agreement between the LIBEAM data and the EFIT calculation with no particular structure in either case.

In contrast, the measured  $H$ -mode pitch angle shows a substantially different character from the  $L$ -mode data,

$$\mu_0 j_{\text{Tor}} = B_{\text{VIEW}} \frac{\left[ \frac{\partial \tan \theta_B}{\partial z} - \frac{\tan^2 \theta_B}{R} - \tan \theta_B \frac{\partial \tan \theta_B}{\partial R} \right]}{\left[ \cos \theta_V + \sin \theta_V (\tan \theta_B) \right]} + B_{\text{VIEW}} \frac{\left[ \frac{\partial \cos \theta_V}{\partial R} + \frac{\partial \sin \theta_V}{\partial R} \tan \theta_B + \sin \theta_V \frac{\partial \tan \theta_B}{\partial R} \right] [1 + \tan^2 \theta_B]}{\left[ \cos \theta_V + \sin \theta_V (\tan \theta_B) \right]^2} - \frac{\partial B_{\text{VIEW}}}{\partial R} \times \left[ \frac{1 + \tan^2 \theta_B}{\cos \theta_V + \sin \theta_V (\tan \theta_B)} \right]. \quad (3)$$

Figure 4 shows the result of such a calculation for the  $L$ -mode and  $H$ -mode lithium beam measurements shown in Fig. 3, using the data points in the range 218–226 cm. For the  $H$ -mode case, the results are striking. We find a very peaked current distribution near the last closed flux surface with current densities in the range 1 to 2 MA/m<sup>2</sup>. The location of the peak is coincident with the location of the peak of  $\nabla Pe$  to within the present spatial resolution, about a centimeter given field mapping uncertainties and known toroidal offsets in the DIII-D coil set. The error shown is dominated by the uncertainty in estimating the derivative terms in Eq. (3), as opposed to statistical error.

These data are taken immediately prior to the occurrence of type 1 ELMs where the same total plasma current exists but the edge pressure gradient has risen to a very high value ( $\sim 50$  times that of the  $L$ -mode phase). Just inside the last closed flux surface, there is a marked increase in the measured pitch angle in the  $H$ -mode as compared to the  $L$ -mode data. The large variation in the lithium beam pitch angle between 2.22 and 2.245 m is indicative of a substantial plasma current, exactly where the large pressure gradient exists; in contrast, the region inwards of 2.19 m shows little variation and is statistically indistinguishable from either the  $L$ -mode data or the EFIT data.

Using Ampère's law, the geometry of the flux surfaces, and the fact that the magnetic field is divergence free, the toroidal current density can be calculated directly from the measured  $B_{\text{VIEW}}$  values and the known spatial calibration. From Ampère's law:

$$\mu_0 j = \nabla \times B \rightarrow \mu_0 j_{\text{Tor}} = \frac{\partial B_R}{\partial z} - \frac{\partial B_z}{\partial R}. \quad (1)$$

By the appropriate substitutions we may express (1) in terms of the measured value

$$\begin{aligned} B_{\text{VIEW}} &= B_z \cos \theta_V \\ &\quad + B_R \sin \theta_V \\ &= B_z (\cos \theta_V + \sin \theta_V \tan \theta_B), \end{aligned} \quad (2)$$

where  $\theta_V$  is the inclination angle of the  $i$ th view chord, obtained from the spatial calibration, and  $\theta_B$  is the magnetic inclination angle  $\tan \theta_B = B_R/B_z$ . We choose this particular parametrization because both the total magnetic field and the quantity  $\tan \theta_B$  are very weakly dependent on the particular current density and can be taken from an initial EFIT reconstruction. Using these relationships we can solve for  $j_{\text{Tor}}(r)$  solely in terms of  $B_{\text{VIEW}}$ , its derivating along the beam trajectory, and the estimated value of  $\tan \theta_B$  and its derivatives:

The spacing of the measurement locations is more than adequate to resolve the width of the current peak.

For comparison with the experimentally derived  $j_{\text{Tor}}$  we also plot the result of an initial bootstrap current calculation for the ELM-free  $H$ -mode case. In Fig. 4, the dashed curve is the predicted toroidal current density from an equilibrium reconstruction using the measured pressure profile and a current density near the edge ( $R > 2.22$  m) constrained by a bootstrap current which is calculated from the measured plasma pressure profiles using the NCLASS code [17]. Given the limitations of the theory mentioned previously and the probable mapping

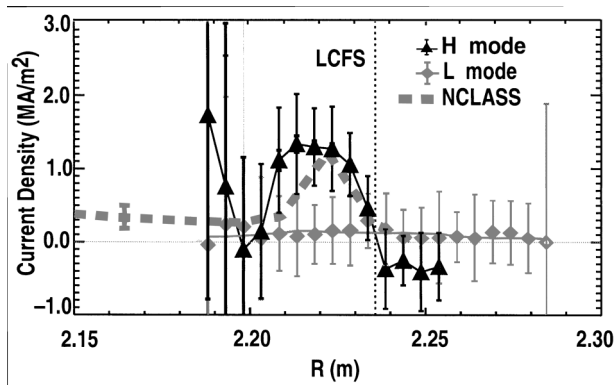


FIG. 4. Calculation of edge current density from LIBEAM pitch angle profile measurements for shot 115114 during the  $L$ -mode (gray) and late ELM-free  $H$ -mode (black) phase just before the collapse of the pedestal pressure, showing a large current peak in the pedestal region. Also shown for comparison is the toroidal current density calculated from a bootstrap constrained fit (dashed curve) for the  $H$ -mode phase. The last closed flux surface from EFIT on the LIBEAM trajectory is indicated by the dotted line.

error from the reconstruction, we find reasonable agreement between the two. The peaks are of similar magnitude and in approximately the same location. The width of the current peak from the lithium beam data is somewhat broader but the decrease in signal in the open field region along with the present spatial resolution in the equilibrium reconstruction makes an exact comparison difficult. In any event, the measured values of  $j_{\text{Tor}}(r)$  are large enough to be important for the theory of edge stability described previously. Preliminary ELITE runs using the equilibria generated above indicate stability for modes having  $n$  below 15, marginal stability for modes of medium  $n(20-25)$ , and instability for modes having  $n = 30-35$  [18]. This behavior is consistent with the approach to ELM onset expected from the stability model.

Figure 5 shows a similar calculation of  $j_{\text{Tor}}$  for shot 115099. This was a discharge having a “quiescent”  $H$ -mode ( $QH$ -mode) phase, characterized by an edge having little or no ELM activity yet possessing an appreciable edge pressure gradient [19]. The measured current distribution is similar in shape and location to that found in the ELM-free  $H$ -mode case. The ratio of the magnitudes is roughly equivalent to the ratio of the pressure gradients for the two cases.

In conclusion, we have observed large localized currents in the edge of DIII-D discharges ( $H$  mode and  $QH$  mode) which are correlated with large edge pressure gradients. The lithium beam polarimetry measurements have sufficient spatial resolution to locate and resolve the peak in the edge  $j(r)$ . The magnitude of the current is sufficient to be important in the present MHD models. We expect that with more detailed analysis (including more

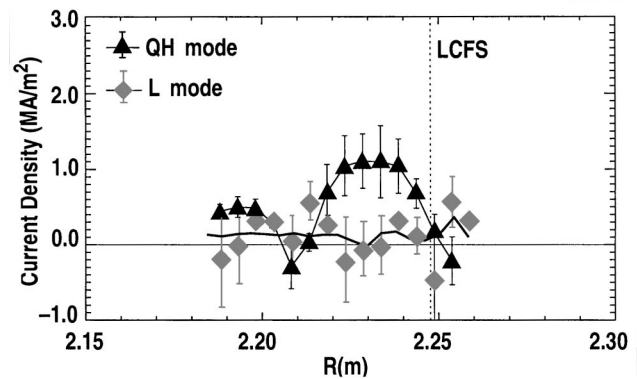


FIG. 5. Calculated edge current density for shot 115099 during the  $QH$ -mode and  $L$ -mode phases.

precise, iterated equilibrium reconstructions to better identify the plasma edge) that this new data will allow us to evaluate (and validate) specific results from edge bootstrap models and stability code predictions for a variety of plasma edge conditions.

This work was supported under the U.S. Department of Energy Contract No. DE-AC03-99ER54463. The authors would like to thank R. J. Groebner, P. B. Snyder, C. C. Petty, M. A. Mahdavi, H. E. St. John, and K. H. Burrell for many useful discussions. We are grateful for the continuing encouragement and support of T. S. Taylor and R. D. Stambaugh.

- 
- [1] S. P. Hirshman, *Phys. Fluids* **31**, 3150 (1988).
  - [2] O. Sauter, C. Angioni, and Y. R. Lin-Liu, *Phys. Plasmas* **6**, 2834 (1999).
  - [3] R. L. Miller *et al.*, *Plasma Phys. Controlled Fusion* **40**, 753 (1998).
  - [4] H. R. Wilson *et al.*, *Phys. Plasmas* **6**, 873 (1999).
  - [5] G. L. Jackson *et al.*, *Phys. Rev. Lett.* **167**, 3098 (1991).
  - [6] T. H. Osborne *et al.*, *J. Nucl. Mater.* **266-269**, 131 (1999).
  - [7] J. R. Ferron *et al.*, *Phys. Plasmas* **7**, 1976 (2000).
  - [8] L. L. Lao *et al.*, *Nucl. Fusion* **41**, 295 (2001).
  - [9] P. B. Snyder and H. R. Wilson, *Contrib. Plasma Phys.* **42**, 258 (2002).
  - [10] P. B. Snyder *et al.*, *Phys. Plasmas* **9**, 2037 (2002).
  - [11] H. R. Wilson *et al.*, *Phys. Plasmas* **9**, 1277 (2002).
  - [12] L. L. Lao *et al.*, *Nucl. Fusion* **30**, 1035 (1990).
  - [13] D. M. Thomas, *Rev. Sci. Instrum.* **66**, 806 (1995).
  - [14] D. M. Thomas *et al.*, *Advanced Diagnostics for Magnetic and Inertial Fusion*, edited by P. E. Stott *et al.* (Kluwer Academic/Plenum Publishers, New York, 2002), p. 319.
  - [15] D. M. Thomas, *Rev. Sci. Instrum.* **74**, 1541 (2003).
  - [16] C. C. Petty *et al.*, *Nucl. Fusion* **42**, 1124 (2002).
  - [17] W. A. Houlberg, K. C. Shaing, S. P. Hirshman, and M. C. Zarnstorff, *Phys. Plasmas* **4**, 3230 (1997).
  - [18] P. B. Snyder (private communication).
  - [19] K. H. Burrell *et al.*, *Plasma Phys. Controlled Fusion* **44**, A253 (2002).